Theoretical studies on the contact distance dependence of the electron transfer reactivity of the ClO/ClO$^+$ coupling system

Shihai Yan,[ab] Yuxiang Bu*[abc] and Lixiang Sun[b]

[a] *Institute of Theoretical Chemistry, Shandong University, Jinan 250100, P. R. China. E-mail: byx@sdu.edu.cn*
[b] *Department of Chemistry, Qufu Normal University, Qufu 273165, P. R. China*
[c] *State Key Laboratory of Rare-earth Materials and their Applications, Peking University, Beijing 800871, P.R. China*

Received (in Montpellier, France) 24th October 2002, Accepted 30th January 2003
First published as an Advance Article on the web 14th May 2003

The structures and properties of ClO, ClO$^+$ and their coupling system are studied with *ab initio* (HF and MP2) and density functional theory (DFT: B3LYP, B3P86, B3PW91) employing the 6-311+G(3df) basis set. Results indicate that there are five possible stable coupling complexes, which correspond to generous minima on the global potential energy surfaces (PES). The most stable coupling complex is EC.3 (C_s, ^{2}A′) in which there is one O–O linkage and two anti-disposed Cl atoms. The stabilization energies are calculated to be 35.78 (EC.1: C_{2h}, ^2B_g), 58.34 (EC.2: C_{2v}, $^2A_2$), 61.72 (EC.3: C_s, ^{2}A′), 59.07 (EC.4: C_{2h}, ^2B_g) and 25.21 (EC.5: C_{2h}, ^2A_g) kcal·mol^{-1} at the B3LYP/6-311+G(3df) level with correction of the basis set superposition error (BSSE); the stability order of these encounter complexes is EC.3 > EC.4 > EC.2 > EC.1 > EC.5. On the basis of the five encounter complexes, five coupling modes are designed for the electron transfer reactivity of this system, in which the contact distance between the two directly linked atoms is defined as the reaction coordinate. The dissociation energy curves at the activated states and the corresponding activation energies of these five coupling modes are obtained and also are compared at the B3LYP/6-311+G(3df) and MP2/6-311+G* levels. The inapplicability of DFT methods in predicting the energy curves, especially with long contact distances, is also discussed in this paper; the DFT methods give an abnormal behavior for the dissociation of the complexes due to the "inverse symmetry breaking" problem. On the basis of the golden rule of time-dependent perturbation theory, the electron transfer reactivity and the contact distance dependences of the various electron transfer kinetics parameters (the activation energy, the coupling matrix element, *etc.*) have been analyzed at the MP2(full)/6-311+G* level. The electron transfer can take place over a range of contact distances, but the most effective coupling distance perhaps corresponds to only a small range of distances. The coupling orientation analysis also indicates that the most favorable coupling mode for the electron transfer does not always correspond to the mechanism for the formation of the most stable encounter complex. Some highly energetic coupling modes perhaps favor the electron transfer reaction.

1. Introduction

The electron transfer (ET) reaction has been proved to be one of the fundamental processes in chemistry and biology, playing a pivotal role in photosynthesis, respiration, and many enzymatic, inorganic, and organic reactions.[1–4] In recent years, it has attracted much attention from researchers all over the world. Many important results have indicated that the electron transfer mechanism depends strongly on the interaction mode, including the contact distance and relative orientation between the donor and acceptor active centers. There are many factors that effectively affect the coupling modes and the electron transfer reaction kinetics. In particular, the coupling interaction is a key factor to determine the electron transfer rate and mechanism. In addition, the structural activation and reorganization of the reacting complexes (the encounter complex or the precursor complex) are other important factors determining the electron transfer rate. Obviously, the coupling interaction strength between the donor and the acceptor is closely related to the combination mode, the contact distance and the properties of the donor and the acceptor systems. However, many recent investigations regarding the various interactions have indicated that there is a range of intermolecular weak interactions occurring among biological macromolecules, materials' macromolecules and interstellar molecules. In general, these systems with a weak interaction are structurally slightly stable, meta-stable or unstable, so they are not easily observed experimentally. Investigations on these kinds of weak interactions thus present an important challenge to theoreticians as high-quality treatments with electron correlation and large basis sets are needed in the theoretical analysis of these systems.[5] ET is important for understanding and controlling chemical reactions, the classical theory of chemical reactions neing based on the concept of an activated complex. Donor-accepter complexes, excited-state charge transfer complexes and ion pairs provide the gas-phase "laboratories" where ET, energy transfer, and their interplay may be explored independently of the complications brought about by the presence of a solvent.[6]

In general, ET can occur over a large range of contact distance, although there is a maximum reaction probability for each ET system at an optimum contact distance. However, for a real system and especially for a gaseous system, since the donor-acceptor groups are generally active, structural constraints perhaps do not assure the donor-acceptor species the optimum interaction mode favoring ET. The coupling mode

 DOI: 10.1039/b210488a

for ET or proton transfer may vary as the surroundings change. Therefore, it is very interesting to investigate the ET reactivity of a system at different contact distances and the effect of the coupling mode on the ET mechanism. However, although there are many publications that focus on the ET reactivity of various systems, there seriously lacks studies on the coupling mode (including contact distance and orientation, *etc.*) dependence of the ET reactivity of any system.

In view of the computational cost at the wave-function-correlated *ab initio* theoretical levels, computational methods based on density functional theory (DFT) are widely used. These methods can predict relatively accurate molecular structures and vibrational frequencies with moderate computational effort for the equilibrium systems. However, for the ET systems mentioned above, the ET must not require the donor and the acceptor to be in their most favorable geometries. Once the ET condition is met, the transfer may occur with a considerable probability regardless of whether the coupling system is at the equilibrium geometry or in a non-equilibrium geometry. So in order to explore the electron transfer reactivity of the system at far from equilibrium geometry, the potential surface of the system far from equilibrium is necessarily determined. Therefore, this work also presents a challenge for theoretical calculation methods, which can be suitable or not for calculations on systems at geometries far from equilibrium.

A recent study has indicated that the energy curves obtained with some DFT methods (such as B3LYP, B3P86, *etc.*) present an abnormal dissociation behavior. This abnormal behavior was first reported by Bally and Sastry in 1997[7] and was recognized to be due to the "inverse symmetry breaking" problem. In view of this consideration, another goal of this paper is to check the applicability of DFT methods and the wave-function-correlated *ab initio* methods in predicting energy curves, especially at long contact distances, and to test the abnormal behavior if exhibited by the system. Through the investigations, the following two points should be stressed. Firstly, both these methods (B3LYP and MP2) are suitable for computational studies on the equilibrium systems. Secondly, the DFT method (B3LYP) is inappropriate for investigating the systematic electronic transfer reactivity due to the "inverse symmetry breaking" problem, especially at long contact distances, but the MP2 method can yield good results. So both the DFT and Møller–Plesset methods are used in this work but in different situations.

Because of the importance of the oxides and peroxides of chlorine in upper atmosphere chemistry (it is believed that they play a key role in ozone depletion over the Antarctic in spring), they have aroused broad interest among chemists and both experimental studies and theoretical calculations on the chemical and physical properties[8–16] of isomeric Cl_2O_2 and its fragments have been carried out. In the experimental area, the thermodynamic properties of gaseous Cl_2O_2 and its fragments have been determined, and the ionization energies of ClO and Cl_2O_2 have also been reported.[17] On the other hand, various theoretical investigations have also been performed. Those include studies on the structures and properties of Cl_2O_2 isomers,[16,18] ClOO,[19] ClO_2^+,[20] [ClO_x, ClO_x^- ($x = 1$–4) and Cl_2O_x ($x = 1$–8)],[21] the pressure dependence and the metastable state formation in photolysis of dichloride monoxide (Cl_2O),[22] and the reaction mechanisms[23] of Cl_2O_2, $Cl_2O_2^+$, $O_3 + Cl$,[24] and $ClOOCl^-$,[25,26] *etc.*

In our previous work,[27] the geometric properties and the electron transfer at the equilibrium geometries of the encounter complexes for the $ClO/ClO^-/ClO^+$ systems have been discussed in detail. But up to now there have not been any publications that focused on the studies of the dependence on the contact distance of the electron transfer reactivity of these systems. Therefore, taking the ClO/ClO^+ pair as a model species, the accurate descriptions of the kinetics parameters of the self-exchange ET reaction will be made, and the contact distance dependence of various kinetics parameters such as the activation energy, the coupling matrix element and the electron transfer rate of the ClO/ClO^+ coupling system will be analyzed in this paper. The suitable theoretical levels for these kinds of investigations will be also evaluated.

2. Theoretical schemes

2.1 Simple description of the theoretical model

Tthe unimolecular rate constant of the electron transfer step can be determined by quantum mechanical methods. There are many quantum mechanical theories that have been used successfully in discussing the relationship between the ET and the correlative parameters.[28,29] Among these theories, the simplest quantum mechanical method for describing the rate of a transition is time-dependent perturbation theory. The golden rule is an excellent tool, which has been successfully used in dealing with a variety of systems, such as the ET reaction in O_2/O_2^-, $M^{2+}OH_2/M^{3+}OH_2$ (M = V, C_r and Mn) and the hydrogen transfer tunneling reaction.[5,30–35] The electron transfer rate is expressed in a particularly simple form according to the golden rule as:

$$k_{et}(R_{a\text{–}b}) = (4\pi^2/h)|H_{if}(R_{a\text{–}b})|^2\rho(E_f,\ R_{a\text{–}b}) \qquad (1)$$

where H_{if} denotes the coupling interaction between the initial $|i>$ and final $|f>$ states, with an energy difference ΔE. Therefore, the linear shape function, $\rho(E_f)$, represents energy conservation, such that in actual calculations ρ (0) represents the density of the initial state $|i>$ (within the limits of the uncertainty principle) with the same energy as the final state $|f>$.

Obviously, from eqn. (1) it can be easily concluded that the coupling matrix element, H_{if}, is one of the key quantities for the calculation of the electron transfer rate. Actually it also represents the energy difference between the non-adiabatic activation state (at the crossing point) and the adiabatic activation state (at the actual transition state), so it can be expressed as:

$$H_{if}(R_{a\text{–}b}) = E_d - E_a(R_{a\text{–}b}) \qquad (2)$$

where E_d denotes the non-adiabatic activation energy, which is also the energy of the reaction system at the crossing-point; $E_a(R_{a\text{–}b})$ denotes the adiabatic activation energy when the contact distance of the two reaction species is $R_{a\text{–}b}$.

2.1.1 Activation energy. When the electron transfer takes place, the energy conservation principle requires that the energy of the activated complex before the electron transfer should be equal to the energy after the electron transfer, namely, $E_{ClO}(r_a^*) + E_{ClO^+}(r_b^*) = E_{ClO^+}(r_a^*) + E_{ClO}(r_b^*)$. Since ClO and ClO^+ are two different species, their structures and properties must be distinguished from each other, accordingly, the equation requests that r_a^* should be equal to r_b^*. The activation parameters may be obtained using the minimization method. Therefore, the energy of the system $ClO\cdots ClO^+$ at the activated state may be expressed as:

$$E_a^* = E_{ClO}(r_a^*) + E_{ClO^+}(r_a^*) \qquad (3)$$

Obviously eqn. (3) represents the energy curve formed in the crossing between the two nonadiabatic potential energy surfaces corresponding to the initial and the final states of the electron transfer, respectively. Thus, the adiabatic activation energy, E_a, is easily obtained by subtracting the energy of each encounter complex from the corresponding energy at the activated state:

$$E_a(R_{a\text{–}b}) = E_{ClO\cdots ClO^+}(r_a^*,\ r_a^*,\ R_{a\text{–}b}) - E_{ClO\cdots ClO^+}(r_{ClO},\ r_{ClO^+},\ R_{a\text{–}b}) \qquad (4)$$

Actually, this state intuitively represents the geometry at which the electron transfer is likely to take place.

Similarly, the diabatic activation energy, E_d, is then obtained by subtracting the energies of the two isolated molecular fragment species [ClO($^2\Pi$) and $ClO^+(^1\Sigma)$] at their own equilibrium geometries from the energy of the reacting system at the activation state:

$$E_d = E_{ClO}(r_a^*) + E_{ClO^+}(r_a^*) - E_{ClO}(r_a) - E_{ClO^+}(r_b) \quad (5)$$

2.1.2 The electronic coupling matrix element. The electronic coupling matrix element denotes the energy lowering caused by the coupling between the initial and the final states of the electron transfer process. Because there is a process of stabilization (E_s), the electronic coupling matrix element may be obtained from:

$$H_{if}(R_{a-b}) = E_{ClO}(r_a^*) + E_{ClO^+}(r_a^*) - E_{ClO\cdots ClO^+}(r_a^*, r_a^*, R_{a-b}) + E_s \quad (6)$$

2.1.3 The final state density. In eqn. (1), $\rho(E_f)$ denotes the final state density. There must be three states in the acceptor ion identifiable with states having the same energy as that of the initial state, these states having the energy $E_f + \Delta E$, E_f and $E_f - \Delta E$, so there are three states per $2\Delta E$. ΔE is the difference between the initial state and the final state energies and can be taken as the uncertainty in the energy of the electron, $\Delta E = (\Delta p)^2/2m_e$. Hence the maximum value of the state density is:

$$\rho(E_f, R_{a-b}) = 3m_e/(\Delta p)^2 = 3m_e(\Delta x)^2/h^2 \quad (7)$$

where Δx is the uncertainty in the position of an electron across the interface and is approximately equal to the contact distance (R_{a-b}).

2.2 The computational methods

In this work, all calculations are carried out using the Gaussian 94 package of programs, version D.4.[36] For this system, the geometry optimizations of the monomers [ClO($X^2\Pi$) and $ClO^+(X^1\Sigma)$] and the corresponding encounter complex ($ClO\cdots ClO^+$) were performed using Hartree–Fock, Becke's three-parameter hybrid functional with Perdew 86, Becke's three-parameter hybrid functional with Perdew/Wang 91, Becke's three-parameter hybrid functional using the LYP correlation functional and the unrestricted second-order Møller–Plesset perturbation theory, with a fairly large basis set having two sets of polarization functions [UHF, UB3P86, UB3LYP, UB3PW91)/6-311+G(3df) and UMP2(full)/6-311+G*]. The optimized geometrical structures of the isolated molecular species and the corresponding encounter complexes at the B3LYP level employing the 6-311+G(3df) basis set are shown in Fig. 1. The stabilization energy has also been corrected using the counterpoise corrections method for the basis set superposition error (BSSE).[37] But in view of the inapplicability of DFT methods in predicting the energy curves, especially with long contact distances for the reasons discussed above, the dependence on the contact distance of the activation energy $E_a(R_{a-b})$, the electronic coupling matrix element $H_{if}(R_{a-b})$ and the final state density $\rho(E_f, R_{a-b})$, as well as the corresponding electron transfer rate $k_{et}(R_{a-b})$ of the five chosen coupling modes are determined in terms of *ab initio* MP2 calculated quantities. In order to show further the unsuitability of the DFT method, the contact distance dependence of $E_a(R_{a-b})$ is also presented.

Substitution of eqn. (7) into eqn. (1) yields the modified equation:

$$k_{et}(R_{a-b}) = (4\pi^2/h)\,|H_{if}(R_{a-b})|^2 \cdot 3m_e\,(\Delta x)^2/h^2 \quad (8)$$

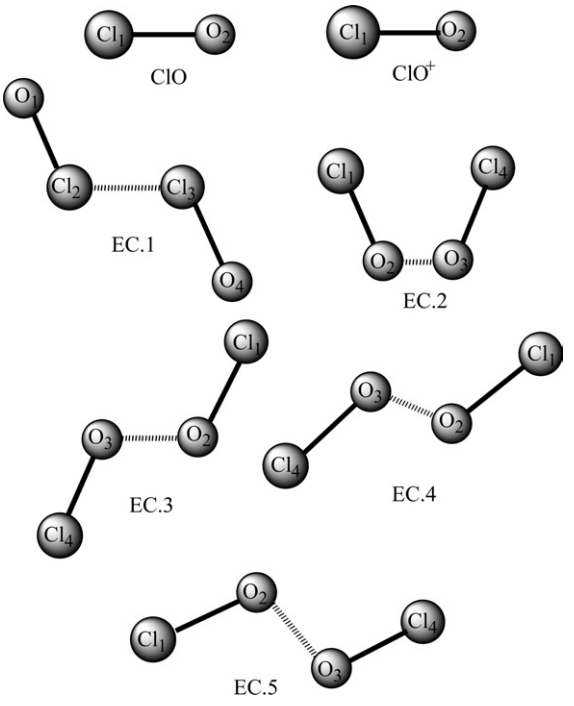

Fig. 1 The geometrical structures of the isolated molecular species and the five stable encounter complexes at the B3LYP/6-311+(3df) level.

so the contact distance dependence of the coupling matrix element, the final state density and the electron transfer rate for the encounter complex of the $ClO\cdots ClO^+$ system are easily calculated using the MP2 method employing 6-311+G* basis set.

In order to obtain the corresponding smooth potential energy curves for the calculations of the activation parameters and activation energies, the calculated energy points are fitted to a third-degree polynomial in r, for the polynomial; the correlation coefficient, R^2, for the fitting accuracy is close to 1.0, indicating that the fitted curves from the calculated data are good. The energy points are also fitted to a fourth-degree polynomial as a check for possible error in the fitting procedure. The fitted potential energy curve function may be expressed as:

$$E(r) = a_0 + a_1 r + a_2 r^2 + a_3 r^3 + \ldots + a_n r^n \quad (9)$$

The data of the fitting parameters (a_0–a_3) obtained from the B3LYP/6-311+G(3df) and MP2/6-311+G* methods are given in Table 1, from which it easily can be seen that the difference between the coefficients of the fourth-degree polynomial and the third-degree polynomial about r is very small, and no substantial changes were observed in the results determined by using the third-order polynomial about r compared with those using the fourth-order polynomial. Only the value of R^2 for EC.3 is small, but it is more suitable for a logarithmic equation and the R^2 is then 0.9711, so it is reliable too.

3. Results and discussion

3.1 The isolated species

It is very important to first analyze the relevant electronic structures and properties of the isolated species before discussing the electron transfer reactivity and some kinetic properties of the self-exchange ET reaction system, ClO/ClO^+.

Some structural parameters and properties of the isolated molecular species [$ClO^+(X^1\Sigma)$ and $ClO(X^2\Pi)$] are listed in Table 2, which are obtained at the given levels. From this table it can be seen that the optimized r parameter of ClO and ClO^+ at the B3LYP/6-311+G(3df) level is 1.5756 and 1.4729 Å,

Table 1 The fitted potential parameters for the activated state energy curves [eqn. (9)] of the different coupling modes from the B3LYP/6-311+G(3df) and MP2/6-311+G* calculated energy data (the units for a_i are a.u. Å^{-i}, i = 0,1,2,3)[a]

	B3LYP					MP2				
	a_3	a_2	a_1	a_0	R^2	a_3	a_2	a_1	a_0	R^2
ClO		0.7073	−2.2261	−533.61	0.9995		0.7285	−2.3405	−532.4	0.9999
	−1.3688	7.0105	−11.898	−528.67	1.0014	−1.2494	6.5253	−11.303	−527.78	0.9953
ClO^+		0.6418	−1.8777	−533.54	0.9998		0.5691	−1.5842	−532.71	1.0000
	−1.3849	7.0192	−11.63	−528.53	0.9997	−1.5463	7.7433	−12.677	−526.99	1.0002
EC.1		−0.0123	0.0947	−1070.5	0.9987		−0.0008	0.018	−1067.9	0.8618
	0.0019	−0.0292	0.1442	−1070.5	0.9992	0.00002	−0.0012	0.0201	−1067.9	0.8616
EC.2		−0.017	0.1274	−1070.5	0.9966		−0.0036	0.0593	−1068.1	0.951
	0.0052	−0.0636	0.2633	−1070.7	0.9997	0.0006	−0.015	0.1201	−1068.1	0.9756
EC.3		0.0018	−0.0012	−1070.3	0.4784		−0.0022	0.0398	−1068.0	0.9183
	−0.0151	0.1325	−0.3678	−1070.0	0.5511	0.0005	0.0116	0.0991	−1068.1	0.9872
EC.4		−0.013	0.1053	−1070.5	0.9921		−0.0013	0.0225	−1067.9	0.8431
	−0.0106	0.0634	−0.0704	−1070.4	0.9974	−0.0002	0.0022	0.0049	−1067.9	0.8485
EC.5		−0.0013	0.0198	−1070.4	0.8275		−0.004	0.0682	−1068.1	0.8722
	0.0003	−0.0063	0.0475	−1070.4	0.9279	0.0006	−0.0145	0.1221	−1068.2	0.9001

[a] Note: for each species, the data in the first line denote the coefficients of the third-order polynomial, and the data in the second line denote those of the fourth-order polynomial about r.

respectively. At the same level, the bond length of ClO^- is also obtained, which is 1.6904 Å. Compared with the experiment data of 1.5696 Åfor ClO[38] and 1.691 Å for ClO^-,[39] the difference is only 0.006 and 0.0006 Å, respectively. It should be pointed out that the bond length of ClO^+ calculated using the MP2 method is 1.4729 Å, just equal to the B3LYP result, and the bond length difference of ClO obtained between the MP2 and B3LYP methods is very small, only 0.0263 Å. Thus the reliability of the B3LYP method is well-established for the prediction of the structure, the heat of formation and the vibrational properties of molecules.[24] Through a comparison of the calculated frequency [861.8 cm^{-1} for B3LYP/6-311+G(3df)] and the experimental value (866 cm^{-1}),[24] the same conclusion can be drawn. Another illustration of the reliability of the B3LYP/6-311+G(3df) method is provided by a comparison (in Table 3) of the theoretical and experimental values of the equilibrium internuclear distance r_e, the harmonic stretching frequency ω_e, and the dissociation energy D_e of the dioxygen and dichlorine molecules in their ground state. According to the above analysis, it is easily seen that the B3LYP method gives the best agreement with the experimental data that can be obtained, therefore, the B3LYP method is trustworthy for the optimization of the equilibrium structure. Fromthe comparison of the results obtained by the MP2 and B3LYP methods, it is facilely found that the MP2 method is very reliable for this system.

3.2 Encounter complexes

The encounter complex (EC), also termed the precursor complex, is an important intermediate in the electron transfer process. The geometrical configuration of the EC directly influences both the activation energy of the reaction and the electron coupling matrix element, and further influences the electron transfer rate owing to the fact that the different initial geometries can cause the reacting system to reach different transition states.[5] Therefore, the geometrical configuration of the encounter complex is important for determining the electron transfer rate. For convenience, the five encounter complexes are denoted as EC.1, EC.2, EC.3, EC.4 and EC.5, respectively; they also denote five different coupling modes in discussing the contact distance dependence of the ET kinetics parameters by changing the contact distance between two directly linked atoms (see below for detail). The geometrical structure of EC.1 is different from the four other encounter complexes because the interacting atoms of the two moieties are the chlorine atoms in EC.1, while those in the others are two O atoms

The optimized geometrical structures of the encounter complexes at B3LYP/6-311+G(3df) level are shown in Fig. 1. The corresponding structural parameters, the point group (PG), the electronic state and the zero-point vibrational energy (ZPVE) are listed in Table 4. From Fig. 1 and Table 4, it can be easily be seen that all these five encounter complexes are co-planar and they are symmetric except for EC.3. EC.1 is a C_{2h} symmetry group molecule, and the two ClO moieties are inverted parallel and equal to each other. The dihedral angle is 180.0° and the electronic state of this encounter complex is ^2B_g. The internuclear distance of Cl–O is the shortest one among these five encounter complexes, at only 1.4868 Å, slightly longer by only 0.0139 Å than that in the isolated molecular species, ClO^+. The contact distance of the two moieties is 2.3918 Å between the two Cl atoms. From the above analysis, it can easily be concluded that the net charge population is balanced over the two molecular fragments. Namely, a part

Table 2 The parameters of the isolated species, ClO and ClO^+, optimized at the HF, B3LYP, B3P86, B3PW91 and MP2 levels employing the 6-311+G(3df) basis set

	ClO($X^2\Pi$)			ClO^+($X^1\sum$)		
	R/Å	Freq./ cm^{-1}	ZPVE/ kcal mol^{-1}	R/Å	Freq./ cm^{-1}	ZPVE/ kcal mol^{-1}
HF	1.5812	847.2	1.21	1.421	1310.3	1.87
B3LYP	1.5756	861.8	1.23	1.4729	1124.3	1.61
B3P86	1.5606	899.9	1.29	1.4641	1157.9	1.66
B3PW91	1.5637	891.7	1.27	1.4655	1152.8	1.65
MP2	1.5493			1.4729		

Table 3 The calculated and experimental values of $O_2(^3\sum_g)$ and $Cl_2(^1\sum_g)$ obtained at the B3LYP/6-311+G(3df) level

	$O_2(^3\sum_g)$		$Cl_2(^1\sum_g)$	
	Calcd	Expt[14]	Calcd	Expt[14]
r_e/Å	1.203	1.207	2.010	1.988
ω_e/cm^{-1}	1644.6	1580.36	540.9	564.9
D_e/kcal mol^{-1}	121.64	117.26	58.63	57.13

Table 4 The geometrical parameters (see Fig. 1 for atom numbering), the point group (PG), electronic state (ES), zero-point vibrational energy and stabilization energy (E_s) of the stable encounter complexes optimized at the B3LYP/6-311+G(3df) level

	EC.1	EC.2	EC.3	EC.4	EC.5
R_{12}/Å	1.4868	1.6128	1.5275	1.6353	1.5279
R_{23}/Å	2.3918	1.4693	2.4315	1.4277	2.8008
R_{34}/Å	1.4868	1.6128	1.521	1.6353	1.5279
A_{123}/°	112.0	117.4	117.5	109.6	108.2
A_{234}/°	112.0	117.4	114.0	109.6	108.2
D_{1234}/°	180.0	0.0	180.0	180.0	180.0
PG	C_{2h}	C_{2v}	C_s	C_{2h}	C_{2h}
ES	^2B_g	$^2A_2$	$^2A'$	^2B_g	^2A_g
ZPVE/kcal mol^{-1}	4.05	4.24	3.42	4.21	3.01
E_s/kcal mol^{-1}	35.78	58.34	61.72	59.07	25.21

of the net charge in ClO transfers to ClO^+. The coupling interaction between the donor and the acceptor molecular fragments ($\cdots$ClO and $\cdots ClO^+$) is somewhat weak and the complex structure is floppy. The stabilization energy of EC.1 at the stationary point is 35.78 kcal·mol^{-1} for this encounter complex, only a little bigger than that of EC.5 (25.21 kcal·mol^{-1}), which has the smallest value among these five encounter complexes. EC.2 is C_{2v} symmetrical for the atoms are all in one plane, its electronic state is $^2A_2$ and its dihedral angle is 0.0°, so the repulsion of the two moieties should be notable. The contact distance of the two moieties is much shorter than that in EC.1, at around 1.47 Å. Accordingly, the conclusion can be drawn that the coupling interaction between the acceptor and the donor molecular fragments ($\cdots$ClO and $\cdots ClO^+$) is strong and the complex structure is compact; the energy of this structure should be lower. The Cl–O bond length is 1.6128 Å, longer than the bond lengths of the isolated molecular species. But this kind of change is not the emphasis of the present paper, so they are not discussed further. The geometry of EC.3 is similar to that of EC.1, that is, the two ClO moieties of EC.3 are inverted parallel but the two moieties are not equal to each other, only lying in the same symmetrical plane. From Fig. 1 it easily can be seen that the main difference of EC.3 from EC.1 lies in the O–O linkage in EC.3 and the Cl–Cl linkage in EC.1. EC.3 is also viewed as the anti form of EC.2. The electronic state of EC.3 is $^2A'$, different from EC.1 (^2B_g) and EC.2 ($^2A_2$). The dihedral angle of this encounter complex is 180.0°. Accordingly, there exists only weak repulsion between the two molecular fragment species, so it may be predicted that EC.3 should be slightly more stable than EC.2. The lengths of the Cl–O bond of EC.4 is the longest one among these five encounter complexes, being equal and parallel to each other; the dihedral angle of EC.4 is 180.0°. The symmetry and the electronic state of EC.4 are the same as those of EC.1. The contact distance of the two moieties is only 1.428 Å, the shortest one among these five encounter complexes, therefore, it should be very favorable for electron transfer. Due to the similarity of EC.4 to EC.3, its stability should be close to that of EC.3. EC.5 is also symmetric, the point group and the electronic state are C_{2h} and ^2A_g, respectively. One point that needs to be emphasized is the contact distance of the two moieties at 2.8008 Å, the longest one among these five encounter complexes, so the interaction between them should be the smallest, and energetically it should be the highest-lying one.

The harmonic frequencies and the IR intensities of these encounter complexes obtained using the B3LYP method employing the 6-311+G(3df) basis set are expressed in Table 5. Since there are no imaginary frequencies for the first four ECs, it can easily be seen that all these optimized structures are stable configurations. There exists one imaginary frequency for EC.5, which therefore is not stable. Another point should also be noted, which is that there is one harmonic frequency in each encounter complex whose corresponding value of the IR intensity is very large. This indicates that the infrared absorption is very strong and there is a large peak at that frequency. Another point that should be made is that the discrepancy of the frequencies of EC.2 with the other four encounter complexes is very large. So the frequency analysis of EC.2 is shown in Fig. 2. From this figure, the vibrational modes can be assigned. They are the in-plane sway of the Cl–O bond, the out-of-plane anti-symmetric twist of the O–O bond, the in-plane symmetry flex of the O–O bond, the in-plane swing of the O–O bond, the in-plane symmetric flex of the Cl–O bond and the in-plane asymmetric stretch of the Cl–O bond, respectively. The vibrational modes of other complexes are the same as each other, but they are different from those of EC.2. In order to save space, the vibrational modes of other encounter complexes are not shown in this paper.

At first view of the above analysis, it seems that the formation of the stable encounter complexes has decreased the energy of the encounter complexes in the initial state and further contributes to increase the activation energy, thus forming a barrier for the reaction. Actually, the stabilization of the encounter complexes is attributed to the coupling interaction between the two species. This coupling reduces the energy of the encounter complexes in both the initial and transition states, so it should not lead to a great change in the activation energy.

3.3 Activated states

This may be understood further with the help of Fig. 3, which represents the lower potential energy surface (PES) (shown by a bold solid line) for the case in which a stable encounter complex is formed. The upper PES (fine solid line) represents the case in which no stable encounter complex is formed. If two reacting species cannot form a stable encounter complex, the reaction PES may be expressed by the upper one and the potential well bottom of the reactant state should correspond to the separated ClO and ClO^+ molecules. The actual transition state may be TS1 (with a small reactive coupling), and the non-reactive transition state should be C1 (no coupling). According to Fig. 3, if two reacting species can form a stable encounter complex, the energy of the reacting system should decrease (lower curve in Fig. 3). The potential well bottom of the reactant state should be the stable initial encounter complex. The non-adiabatic transition state (with only initial encounter complex coupling) should be C2 and the actual transition state should be TS2, with further coupling from the initial coupling magnitude. Therefore, the precursor is formed with the initial coupling interaction and this formation of the

Table 5 The frequencies (in cm^{-1}) and the IR intensities (in parentheses and given in km mol^{-1}) of the five encounter complexes optimized using the B3LYP/6-311+G(3df) method

EC.1	64.7 (8.0)	115.7 (8.7)	194.7 (0.0)	355.7 (0.0)	1041.9 (219.5)	1061.7 (0.0)
EC.2	200.7 (0.5)	217.6 (0.0)	415.3 (21.4),	536.3 (2.9)	753.0 (0.1)	845.9 (128.9)
EC.3	58.0 (6.2)	67.9 (4.1)	79.2 (0.2)	249.3 (0.3)	953.7 (420.7)	985.0 (13.1)
EC.4	99.7 (1.7)	241.5 (5.0)	358.7 (0.0)	592.9 (0.0)	748.5 (172.4)	903.5 (0.0)
EC.5	45.7i (5.0)	88.7 (3.4)	101.6 (0.0)	192.0 (0.0)	817.3 (209.3)	909.5 (0.0)

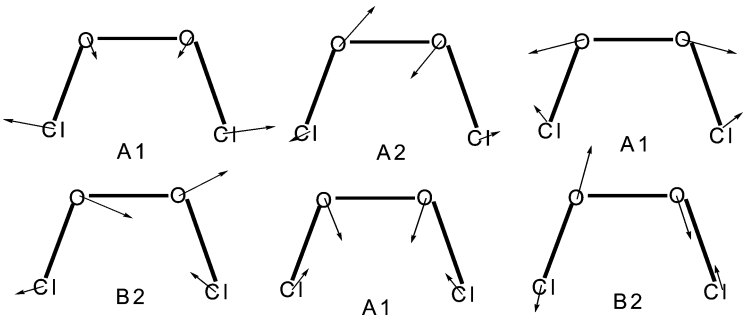

Fig. 2 The six vibrational modes of EC.2 obtained at the B3LYP/6-311+G(3df) level.

precursor decreases both the energy of the reacting system in the initial state and the energy of the reacting system at the crossing point by the same degree (from C1 to C2). The actual transition state should also decrease by the same amount as the initial state coupling from TS1 to TS2. This is to say that the stronger the initial state coupling, the greater the stabilization energy of the initial encounter complex and the greater the decrease of the actual activation energy of the reacting system at the transition state. In brief, the formation of the precursor complex does not obviously affect the activation energy while the effect on the reaction from the activation energy change is smaller than that from the stabilization energy. Therefore, the stability of the precursor facilitates the reaction.[5]

These five encounter complexes imply that the system may experience five different transition states. Namely, there may be five different pathways through which the electron transfers. The activated geometrical parameters (r_a* and r_b*) of the stable encounter complexes at the transition states optimized using the B3LYP method are also indicated in Table 4, from which it can be seen easily that the difference of the bonds in each transition state is small. The Cl–O bond distances of every ClO molecular fragment in these five transition states are equal to each other, *viz.* the bond length r_a* is equal to r_b*. From eqn. (4), the activation energies of these five structures are easily obtained. The potential energy surfaces of the reacting system at the activated state *via* these five coupling modes were scanned. The ET reaction *via* the different contact distances of EC.1, EC.2, EC.3, EC..4 and EC.5 are defined as coupling mode 1, coupling mode 2, coupling mode 3, coupling mode 4 and coupling mode 5. The contact distance (R_{a-b}) dependence of the adiabatic activation energy of these five coupling modes obtained at the B3LYP/6-311+G(3df) and MP2/6-311+G* levels are given in Fig. 4 and Fig. 5, respectively. In these two figures, for the sake of convenience, each curve is plotted by using the relative energies to its minimum energy value, that is to say, the minimum energy of each curve is defined as the zero point, thus these curves have a unified zero-point.

From these two figures, it easily can be seen that the energy curves obtained with the DFT method (B3LYP) exhibit abnormal behavior. This phenomenon was first reported in 1997[7] and it was named "inverse symmetry breaking". Lately the "inverse symmetry breaking" problem was mentioned[40,41] to be a common phenomenon in DFT results for radical ions with two equivalent fragments.

The abnormal results of the DFT method in calculating the contact distance dependence of the dissociation energy can be described from the following two aspects. First of all, the larger the contact distance , the lower the energy. In other words, in the process of scanning the energies of these five coupling complexes at the activated state (even though there exist minima on their energy curves), when R_{a-b} increases from its lowest energy point, the energy calculated using DFT methods initially increases, but after surmounting a fictitious transition state barrier, it decreases. The second abnormal behavior is that whatever the contact distance is, the positive charge and the spin of the three radical cations are delocalized evenly over the two fragments. In fact, there should be a case that when R_{a-b} is large enough, the energy of each complex should be equal to the sum of the total energies of the isolated molecular fragment species, ClO and ClO^+, and the positive charge and the spin of the five radical cations should not be delocalized evenly over the two molecular fragments. From the above analysis, it can be concluded that the energy curves obtained with

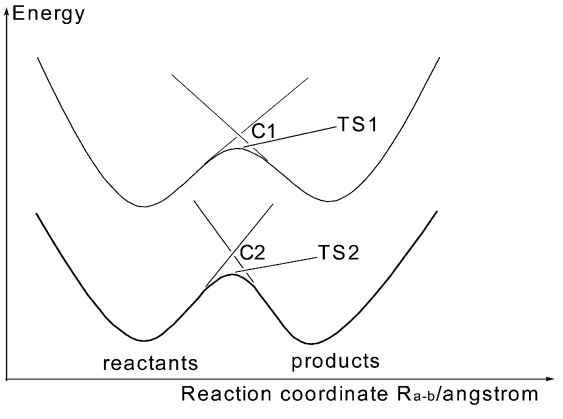

Fig. 3 Potential energy surfaces for the encounter between two species. C1 is the crossing point at which there is no interaction between the two species. TS1 is the corresponding transition state with only the coupling needed for electron transfer. C2 is the crossing point and the state with the largest activation energy while keeping only the weak interaction between the two species; at this point no electron transfer occurs. TS2 represents the actual transition state where there are two coupling interactions (the initial coupling and the additional transition state coupling needed for electron transfer).

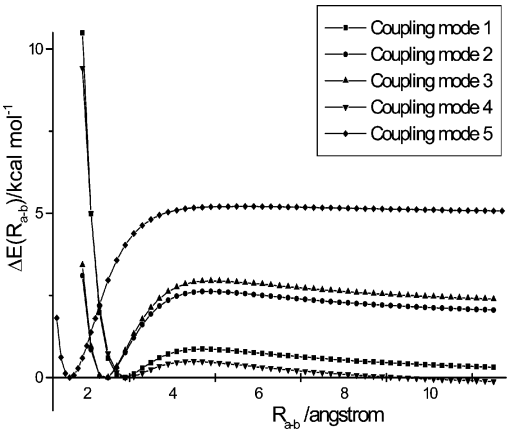

Fig. 4 The energy curves at the activated state reached *via* five coupling modes with respect to different contact distances R_{a-b}, obtained with the B3LYP/6-311+G(3df) method. The relative energy is referred to the energy difference from the minimum energy for each curve.

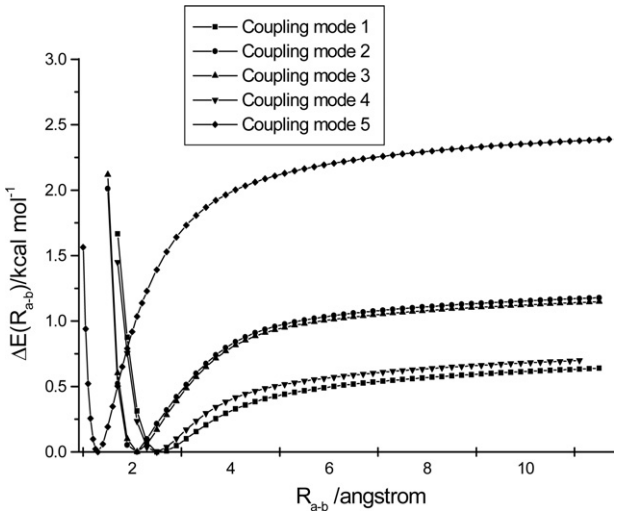

Fig. 5 The energy curves at the activated state reached *via* five coupling modes with respect to different contact distances R_{a-b}, obtained with the MP2/6-311+G* method. The relative energy is referred to the energy difference from the minimum energy for each curve.

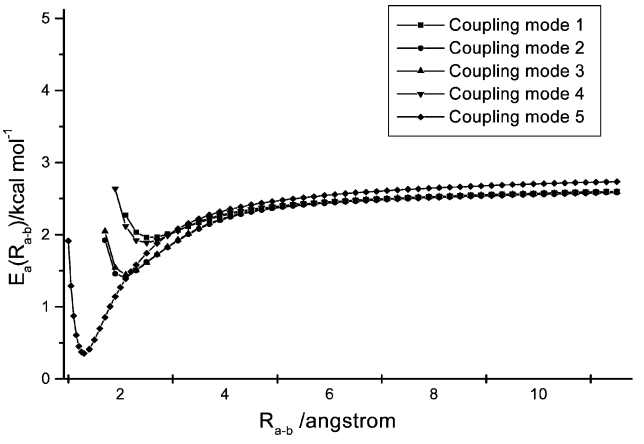

Fig. 6 The contact distance R_{a-b} dependence of the activation energy, $E_a(R_{a-b})$, *via* the five coupling modes obtained with the MP2/6-311+G* method.

DFT methods are definitely unreasonable. Concerning the MP2 method, the energy curves exhibit normal behavior. When the contact distance increases from about 1.5 Å to 11 Å, the systeme energy first decreases, passes through a minimum value, then increases to the dissociation limit. This is obviously reasonable. This phenomenon implies that, although both B3LYP and MP2 methods can yield reliable geometric parameters and energies at the stable equilibrium state for many systems, the former does not work well in predicting those properties for some systems far from equilibrium. So the MP2 method was chosen to scan the energy curves of these five complexes at the activated state in order further to calculate the electronic coupling matrix elements (H_{if}) and the ET rates of the ClO/ClO^+ system at different contact distances.

It is generally known that the lower the total energy of the complex is, the more stable it is. This is to say that the larger the absolute value of the stabilization energy (E_s) is, the more stable is the system. The stabilization energy denotes the energy decrease from the sum of the optimized isolated molecular fragment species to the stable encounter complex, and it is easily obtained by subtracting the summed energy of the two isolated molecular fragment species from the encounter complex. Table 4 lists the relevant stabilization energies obtained using the B3LYP method employing the 6-311+G(3df) standard basis set with the counterpoise corrections method for the basis set superposition error (BSSE).37 The stability order is EC.3 > EC.4 > EC.2 > EC.1 > EC.5. So it can be seen that EC.3 is the most stable configuration and EC.5 is the least stable one among these five encounter complexes. The frequency analysis also confirms the instability of EC.5.

3.4 The ET kinetics parameters

3.4.1. The activation energy. The contact distance (R_{a-b}) dependence of the activation energy $E_a(R_{a-b})$ is displayed in Fig. 6. Up to now, no experimental activation energy for this kind of ET reactions has been reported to our knowledge. From Fig. 6 it can be seen that the activation energy curves of these five coupling modes exhibit a similar characteristic variation. Following the increase of the contact distance, the activation energy deceases firstly, and then increases after passing through a minimum in the activation energy barrier. In detail, for the ET reaction *via* coupling mode 1, when the contact distance is 2.1 Å, the activation energy is 2.27 kcal mol^{-1}. With the contact distance increasing, the activation energy decreases sharply. When the contact distance is 2.5 Å, the activation energy is only 1.96 kcal·mol^{-1}. As the contact distance continuously increases from 2.5 to 11.5 Å, the activation energy increases smoothly in an asymptotic fashion. When $R_{a-b} > 6.0$ Å, the value of the activation energy has increased by about 0.5 kcal·mol^{-1} above the minimum value. For the ET reactions *via* coupling modes 2, 3, 4 and 5, the tendencies are the same as that *via* coupling mode 1 but with different minimum activation energies. For coupling mode 2, the minimum activation energy is 1.40 kcal·mol^{-1} when the contact distance is about 2.1 Å, while for coupling mode 3, the minimum activation energy is 1.44 kcal·mol^{-1} when the contact distance is approximately 2.1 Å also. When the contact distance is about 2.5 Å, the minimum activation energy of coupling mode 4 is 1.88 kcal·mol^{-1}. For coupling mode 5, the minimum activation energy is 0.35 kcal·mol^{-1} when the contact distance is about 1.3 Å. The minimum activation energies *via* these five coupling modes are in the order: coupling mode 5 < coupling mode 2 < coupling mode 3 < coupling mode 4 < coupling mode 1.

Comparison of the activation energy curves of the different coupling modes can give a relative criterion in predicting the ET reactivity at different contact distances. At first, we take the first four coupling modes into account. From Fig. 6 it can be seen that when $R_{a-b} > 2.1$ Å, the activation energies for coupling modes 2 and 3 show the same variation, the only difference being that the activation energy curve for coupling mode 3 is about 0.2 kcal·mol^{-1} higher than that for coupling mode 2. The activation energies of coupling modes 1 and 4 have the same variation for contact distances greater than 2.5 Å, but the activation energy curve for coupling mode 1 is obviously higher than the other three coupling modes. When $R_{a-b} < 2.1$ Å, the curves of coupling modes 2 and 3 have the same variation and almost coincide; they are obviously lower than that of coupling mode 1. The major difference between the curve of coupling mode 1 and those of coupling modes 2 and 3 is that the activation energy curve of the former still decreases when R_{a-b} is just bigger than 2.1 Å, until at 2.5 Å the activation energy reaches its smallest value and then starts to increase. But for those of the latter two modes, at 2.1 Å the curves start to increase. This observation indicates that when the contact distance is smaller than 2.5 Å, coupling modes 2 and 3 are more favorable to ET than coupling modes 1 and 4. But when considering coupling mode 5, the situation is completely dissimilar . The lowest point of the curve is near 1.3 Å, the corresponding activation energy is only 0.35 kcal·mol^{-1}. When the contact distance $R_{a-b} < 1.3$ Å, the activation energy declines rapidly following the increase of the contact distance. When the contact distance $R_{a-b} > 3.3$ Å, the activation energy of coupling mode 5 is bigger than that of the other four, but when the contact distance $R_{a-b} < 2.1$ Å, the activation energy

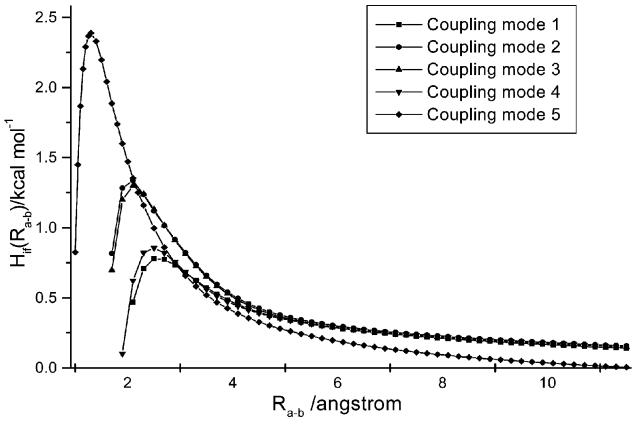

Fig. 7 The contact distance R_{a-b} dependence of the electron coupling matrix element $H_{if}(R_{a-b})$, *via* the five coupling modes obtained with the MP2/6-311+G* method.

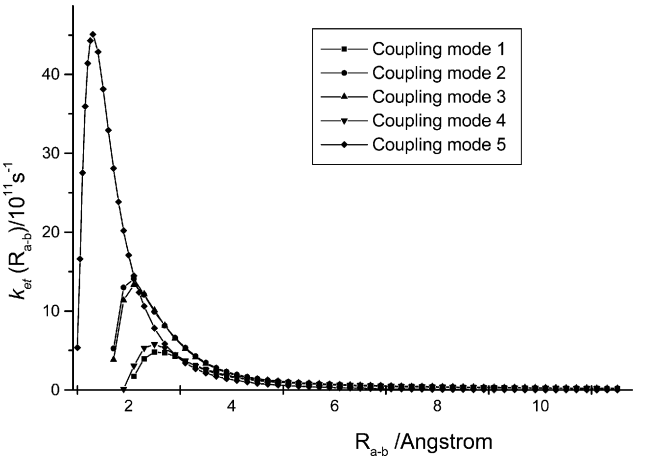

Fig. 8 The contact distance R_{a-b} dependence of the electron transfer rate, $k_{et}(R_{a-b})$, *via* the five coupling modes obtained with the MP2/6-311+G* method.

of this mode is smaller than that of the others. Therefore, from only the viewpoint of the activation energy, it can be predicted that the most favorable coupling mode for ET should be coupling mode 5.

3.4.2. The electronic coupling matrix element. From eqn. (8), it easily can be shown that the ET rate k_{et} strongly depends on the electronic coupling matrix element and it is directly proportional to the square of the electronic coupling matrix element ($|H_{if}|^2$). The larger the electronic coupling matrix element is, the faster the ET rate is. The contact distance dependence of the electronic coupling matrix element is demonstrated in Fig. 7, from which it can be seen that the electronic coupling matrix element curves for the five different coupling modes also exhibit a similar characteristic variation. When the contact distance increases, the coupling matrix element initially increases and, after surmounting a maximum, decreases smoothly. For the ET reaction *via* coupling mode 1, when the contact distance is 2.1 Å the coupling matrix element is only 0.47 kcal·mol^{-1}. The coupling matrix element increases sharply as the contact distance increases. When the contact distance is 2.5 Å, the coupling matrix element is 0.78 kcal·mol^{-1}. For contact distances from 2.5 to 11.5 Å, the coupling matrix element decreases monotonously. In the range of 2.5 Å $< R_{Cl2-Cl3} <$ 5.0 Å, H_{if} changes rapidly its values are greatest in this range of contact distances. We can draw the conclusion that this range, for which the coupling between the donor and the acceptor is strong, is the major zone for the ET reaction. For the ET reaction *via* the other four coupling modes, the variation of the coupling matrix element is the same as that described for coupling mode 1

Similarly, if we analyze the variation of the curves by comparing them at the same contact distance, which coupling mode is more favorable for ET can be determined. From Fig. 7, it can be seen that when $R_{a-b} > 2.7$ Å, these five coupling modes basically have the same variation. The coupling matrix element of coupling mode 5 is the biggest among these five modes, especially when the contact distance lies between 1.3 and 2.5 Å. At infinite contact distance, the five curves basically coincide into one. This is clearly reasonable, because at infinite contact distance, the orbital overlap between the donor and the acceptor is very small and the orientation effect is also not significant, only the electrostatics interaction between the donor and the acceptor plays some role in the coupling, which is similar to that of two classical point-charge spheres. However, when $R_{a-b} < 2.7$ Å, the five curves exhibit significant differences. In the range of 1.9–3.1 Å, coupling modes 2 and 3 have a larger H_{if} than coupling modes 1 and 4 and are more favorable for ET, compared with the latter two modes. The coupling mode 4 lies in the fourth position, while coupling mode 1 is slightly smaller than coupling mode 4. When $R_{a-b} <$ 2.5 Å, the curves of coupling modes 1 and 4 sharply decrease with decreasing R_{a-b}, but the curve of coupling modes 2 and 3 continues to increase until R_{a-b} reaches 2.1 Å, then starts to decrease. This phenomenon implies that for the small contact distances coupling modes 2 and 3 are more favorable to the ET than coupling modes 1 and 4, but the most favorable mode should be coupling mode 5.

3.4.3. The ET rate. According to eqn. (8), it easily can be seen that if the electronic coupling matrix element H_{if} and the final state density ρ have been calculated, the electron transfer rate is very easy to calculate. As we have shown, ρ is only directly proportional to the contact distance and has no dependence on the coupling modes or the orientations. The calculated electron transfer rates using the MP2 method employing the 6-311+G* basis set are given in Fig. 8. It is obvious that when the contact distance is very long, the two isolated species undergo nearly no interaction and thus cannot form the precursor; the electron transfer rate should be very small, from this point the MP2 method is credible. From the factors that influence the rate of ET and Fig 8, it can be seen that upon increasing the contact distance from a very small value, the ET rate increases, and after arriving at a maximum, then decreases. For the ET reaction *via* coupling mode 1, the rate of ET tends to a maximum value (4.80×10^{11} s^{-1}) when $R_{Cl2-Cl3}$is about 2.5 Å where the system has its lowest activation energy (1.96 kcal·mol^{-1}) and biggest coupling matrix element (0.78 kcal·mol^{-1}). Above 3.0 Å, k_{et} rapidly decreases as $R_{Cl2-Cl3}$ increases. When $R_{Cl2-Cl3} > 5.0$ Å, k_{et} decays gently with increasing R and the system has a higher activation energy and lower coupling matrix element. The k_{et} of the ET reaction *via* coupling mode 2 tends to its maximum value (14.09×10^{11}s^{-1}) when R_{O2-O3} is about 2.1 Å. At this point, the corresponding lowest activation energy and biggest coupling matrix element are 1.40 kcal·mol^{-1} and 1.34 kcal·mol^{-1}, respectively. For ET reaction *via* coupling mode 3, k_{et} tends to its maximum value (13.31×10^{11} s^{-1}) when R_{O2-O3} is about 2.2 Å. With increasing contact distance, k_{et} decays rapidly, but this decay slows when $R_{O2-O3} > 5.0$ Å. The electron transfer rate tends to its maximum value (5.77×10^{11} s^{-1}) *via* coupling mode 4 when the contact distance is near to 2.5 Å. The corresponding lowest activation energy and biggest coupling matrix element are 1.88 kcal·mol^{-1} and 2.39 kcal·mol^{-1}, respectively. The ET rate *via* coupling mode 5 is the biggest among these modes and has its maximum value (45.09×10^{11} s^{-1}) when the contact distance is near 1.3 Å. From the above analysis, it easily can be seen that among these five modes, the

largest k_{et} of the ET reaction is that *via* coupling mode 5. The values of k_{et} *via* coupling mode 1 and coupling mode 4 are almost equal. Therefore, the ET occurs mainly in a range of contact distances, $R_{a-b} < 5.0$ Å, and the most favorable coupling mode for the ET is mode 5, the ET occurring chiefly from 1.1 to 3.1 Å; the ET rate of coupling mode 3 is almost equal to that of coupling mode 2

Obviously, this result should be reasonable because this treatment takes into account of the electron transfer probability before the reacting system reaches the activated state in terms of the golden rule principle. It can also be seen that the variation of the electron transfer rate with contact distance has the same behavior as that of the electronic coupling matrix element. When the electronic coupling matrix element is large, the electron transfer rate is also large. When the electronic coupling matrix element is small, the electron transfer rate is also small. According to this analysis, the conclusion can be drawn that the electronic coupling matrix element is one of the most pivotal factors that significantly affect the electron transfer rate.

From the above analysis, it has been shown that it is not always correct that the ET must occur through the most stable coupling mode mechanism. That is to say, in the ClO/ClO^+ system and many other systems, for which the most stable coupling structure could not provide with certainty the most favorable geometry for ET, perhaps some other coupling modes with slightly higher energy are very favorable for ET. Our preliminary investigations on the ET reactivity of some biological molecular systems have indicated this prediction to be reasonable, but it is only a theoretical investigation and needs further experimental exploration.[42]

There are two major aspects in the present treatment of electron transfer that differ from the usual treatment. Above all, it is based on the "nonadiabatic" representation rather than the "adiabatic" representation. In the adiabatic representation, an adiabatic approximation is generally invoked; the adiabatic theory neglects the upper potential energy surface and its nonadiabatic coupling to the lower surface. In the present nonadiabatic treatment, the coupling between the two surfaces, which cross freely in this representation, is adiabatic and can be fully included, whether or not it is weak enough to be treated as a perturbation. For this system ($ClO + ClO^+$), the most favorable ET mode is coupling mode 5. In this mode, the interaction between the accepter and the donor is weak and the molecular structure is floppy, so the nonadiabatic representation is reasonable. Especially for electron transfer far from the equililbrium state, the nonadiabatic representation is very important, whether it is for the most favorable mode 5 or for the other four unfavorable modes.

The second aspect in which our treatment differs from the usual approach is that it implicitly includes all degrees of freedom of the electron transfer. Usually, the electron movement can be accurately depicted in terms of the wavefunctions, but it is impossible to find a one-dimensional potential barrier function for the electron transfer. In this scheme, accurate state-to-state coupling and the spatial movement of the electron are considered directly in terms of the energy formalism.

4. Conclusion

The structural properties and electron transfer reactivity of the ClO/ClO^+ system has been investigated using DFT and MP2 methods at different basis set levels; the main conclusions that can be drawn are the following.

1. There are five different stable coupling modes considered in this paper for this cationic pair. The stability order of the five stable encounter complexes after correction for the BSSE is: encounter complex 3 > encounter complex 4 > encounter complex 2 > encounter complex 1 > encounter complex 5.

2. The inapplicability of DFT methods due to the "inverse symmetry breaking" problem in predicting the dissociation energy curves of the coupling system, especially for those with large contact distances, has been discussed. Results indicate that Møller–Plesset theory can produce normal dissociation behavior for this system and it is suitable for further calculation of the contact distance dependence of the various kinetics parameters (E_a, H_{if}, and the ET rate). Although DFT methods could not give reasonable dissociation behavior for the coupling system far from equilibrium, but they can yield accurate results for the structural properties and ET reactivity at the equilibrium state.

3. The contact distance dependence of E_a, H_{if} and k_{et} has also been discussed. The curves of the contact distance dependence of E_a *via* five coupling modes show the same behavior, they decease firstly then they increase, after passing through the corresponding minimum activation energy barrier. The contact distance dependence of H_{if} and the rate of ET *via* the five coupling modes also show a similar variation. With the contact distance increase from about 1.5 to 11.5 Å, both H_{if} and the rate of ET increase at first, arrive at a maximum, and then decrease. ET occurs chiefly over a range of encounter distances of 1.1 Å $< R_{a-b} <$ 3.1 Å. The most favorable coupling mode for the ET is coupling mode 5, which chiefly occurs in the contact distance range of 1.1 to 3.1 Å, the ET rate of coupling mode 2 is almost equal to that of coupling mode 3. The maximum value of the ET rate is about 45.09×10^{11} s^{-1} *via* coupling mode 5, the corresponding contact distance, R_{O2-O3}, is about 1.3 Å.

4. The results have demonstrated that it is not always true that the ET must occur *via* the most stable coupling mode mechanism. In this system, the coupling modes 3 and 4 are more stable than coupling mode 2, but the more favorable mode for ET is the latter. The most unstable coupling mode is coupling mode 5, but it is the most favorable mode for ET. This observation indicates that perhaps the most stable coupling mode cannot provide the most favorable geometry for ET and that some other coupling modes with slightly higher energies are more favorable for ET. Preliminary investigations on the ET reactivity of some biological molecular systems indicated that this prediction is reasonable, but there are no experimental studies that have focussed on the ET problem in the ClO/ClO^+ system, so it still needs further exploration.

Acknowledgements

This work is supported by NSFC (20273040, 29973022) and by the Foundation for University Key Teacher by the Ministry of Education; support from the Visiting Scholar Foundation of Key Laboratory in the University is also acknowledged.

References

1 P. F. Barbara, T. J. Meyer and M. A. Ratner, *J. Phys. Chem.*, 1996, **100**, 13 148.
2 M. D. Newton and N. Sutin, *Annu. Rev. Phys. Chem.*, 1984, **35**, 437.
3 R. A. Marcus and N. Sutin, *Biochim. Biophys. Acta*, 1985, **811**, 265.
4 R. D. Cannon, *Electron-Transfer Reactions*, Butterworth, London, 1980.
5 Y. X. Bu, D. Zhou, Q. Z. Zhou and C. H. Deng, *J. Mol. Struct. (THEOCHEM)*, 1999, **459**, 177.
6 S. Sergei and A. W. Ralph, *J. Phys. Chem. A*, 2000, **104**, 6314.
7 T. Bally and G. N. Sastry, *J. Phys. Chem. A.*, 1997, **101**, 7923.
8 M. J. Molina and F. S. Rowland, *Nature (London)*, 1974, **249**, 810.
9 S. S. Prasad and W. M. Adams, *J. Photochem.*, 1980, **13**, 243.
10 B. J. Finlayson-Pitts and J. N. Pitts, *Atmospheric Chemistry*, Wiley Interscience, New York, 1986.

11 J. W. Barrett, S. Solomon, E. Richard, R. L. de Zafra, M. Jaramillo, L. Emmons and A. Parrish, *Nature (London)*, 1988, **336**, 455.
12 J. G. Anderson, W. H. Brune, S. A. Lloyd, D. W. Toohey, S. A. Sander, W. L. Starr, M. Loewenstein and J. Podolske, *Geophys. Res.*, 1989, **94**, 11 480.
13 W. H. Brune, J. G. Anderson and K. R. Chan, *J. Geophys. Res.*, 1989, **94**, 16 649.
14 S. P. Sander, R. Friedl and Y. L. Yung, *Science*, 1989, **245**, 1095.
15 V. Vaida, S. Solomon, E. C. Richard, E. Rül and A. Jefferson, *Nature (London)*, 1989, **342**, 405.
16 F. Jensen and J. Oddershede, *J. Phys. Chem.*, 1990, **94**, 2235.
17 S. Abramowitz and M. W. Chase, Jr., *Pure Appl. Chem.*, 1991, **63**, 1449.
18 M. P. McGrath, K. C. Clemitshaw, F. S. Rowland and W. J. Hehre, *J. Phys. Chem.*, 1990, **94**, 6126.
19 V. R. Morris, S. C. Bhatia, T. S. Dibble and J. S. Francisco, *J. Chem. Phys.*, 1996, **104**, 5345.
20 Y. Pak and R. C. Woods, *J. Chem. Phys.*, 1996, **104**, 5547.
21 W. K. Li and C. Y. Ng, *J. Phys. Chem. A.*, 1997, **101**, 113.
22 S. L. Nickolaisen, C. E. Miller, S. P. Sander, M. R. Hand, L. H. Williams and J. S. Francisco, *J. Chem. Phys.*, 1996, **104**, 2857.
23 D. Y. Hwang and A. M. Mebel, *J. Chem. Phys.*, 1998, **109**, 10 847.
24 A. Beltrán, J. Andrés, S. Noury and B. Silvi, *J.Phys. Chem. A.*, 1999, **103**, 3078.
25 A. F. Jalbout, *J. Mol. Struct. (THEOCHEM)*, 2002, **594**, 1.
26 S. H. Yan, Y. X. Bu and K. L. Han, *Sinica Chim. Acta*, 2002, **60**, 1986.
27 S. H. Yan, Y. X. Bu, M. Qin, L. X. Sun and K. L. Han, *J. Mol. Struct. (THEOCHEM)*, 2003, in press.
28 Y. X. Bu and C. H. Deng, *J. Phys. Chem.*, 1996, **100**, 18 093.
29 Y. X. Bu, X. Y. Song and C. H. Deng, *J. Phys. Chem.*, 1999, **103**, 4485.
30 Y. X. Bu, Z. H. Cao and X. Y. Song, *Int. J. Quantum. Chem.*, 1996, **57**, 95.
31 Y. X. Bu, Y. X. Wang, H. T. Sun and C. H. Deng, *J. Mol. Struct. (THEOCHEM)*, 1998, **429**, 143.
32 Y. X. Bu, X. Y. Song and C. B. Liu, *J. Mol. Struct. (THEOCHEM)*, 1999, **489**, 141.
33 Y. X. Bu, X. Y. Song and Y. Nie, *J. Mol. Struct. (THEOCHEM)*, 2000, **530**, 327.
34 Y. X. Bu, Y. J. Ding and C. H. Deng, *J. Mol. Struct.*, 1997, **417**, 69.
35 Y. X. Bu and C. H. Deng, *J. Phys. Chem.*, 1997, **101**, 1198.
36 M. J. Frisch, G. W. Trucks, H. B. Schlegel, P. W. Gill, B. G. Johnson, M. A. Robb, J. R. Cheeseman, T. Keith, G. A. Petersson, J. A. Montgomery, K. Raghavachari, M. A. Al-Laham, V. G. Zakrzewski, J. V. Ortiz, J. B. Foresman, J. Cioslowski, B. B. Stefanov, A. Nanayakkara, M. Challacombe, C. Y. Peng, P. Y. Ayala, W. Chen, M. W. Wong, J. L. Andres, E. S. Replogle, R. Gomperts, R. L. Martin, D. J. Fox, J. S. Binkley, D. J. Defrees, J. Baker, J. P. Stewart, M. Head-Gordon, C. Gonzales, J. A. Pople, Gaussian 94, rev. D.4, Gaussian, Pittsburgh, PA, 1995.
37 C. Lee, W. Yang and R. G. Parr, *Phys. Rev. B*, 1988, **37**, 785.
38 L. Visscher, T. J. Lee and K. G. Dyall, *J. Chem. Phys.*, 1996, **105**, 8773.
39 R. Janoschek, *J. Mol. Struct. (THEOCHEM)*, 1998, **423**, 219.
40 Y. M. Xie, H. F. Schaefer III, X. Y. Fu and R. Z. Liu, *J. Chem. Phys.*, 1999, **111**, 2532.
41 V. Hrouda, M. Roeselova and T. Bally, *J. Phys. Chem. A.*, 1997, **101**, 3925.
42 Q. Sun, Y. X. Bu and M. Qin, *J. Phys. Chem. A*, 2003, **107**, 1584.